

# Gamma Ray Burst Afterglows: A Theoretical Exploration



Mehul Goyal (22B1809)  
Under the guidance of Prof. Varun Bhalerao  
Department of Physics  
Indian Institute of Technology Bombay

# Contents

1	Overview . . . . .	3
1.1	What are Gamma Ray Bursts ? . . . . .	3
1.2	What are GRB Afterglows ? . . . . .	4
1.3	Significance of studying GRBs . . . . .	4
2	Basic Theoretical Framework . . . . .	5
2.1	Relativistic Motion . . . . .	5
2.2	Qualitative description of GRB Model . . . . .	6
3	Afterglow Physics . . . . .	6
3.1	Synchrotron Radiation . . . . .	7
3.2	External Forward Shock Model . . . . .	10
3.3	Jet Effect . . . . .	13
3.4	Reverse Shock Emission . . . . .	15
3.5	Model Parameter Constraints . . . . .	19
4	Extinction Effects . . . . .	20
4.1	What is extinction? . . . . .	20
4.2	Formulation and Host Galaxy Correction . . . . .	21
4.3	Correcting for Galactic Extinction . . . . .	21
4.4	Extinction Correction in GRB 181110A . . . . .	23
5	Modeling of GRB 230204B . . . . .	25
5.1	Calculation of $p$ and ISM vs Wind Environment . . . . .	25
5.2	Forward Shock Model Fit and Parameter Extraction . . . . .	26
6	Conclusion . . . . .	28
6.1	Future Work . . . . .	28

## Abstract

Gamma-ray bursts are one of the most energetic explosions in the Universe, characterized by short-lived gamma-ray prompt emission and a long-lived broadband emission called afterglow. This report begins with an overview of GRBs and their afterglows in Section 1, introducing the fundamental aspects of these astrophysical phenomena. Section 2 outlines the theoretical framework underpinning current GRB models, setting the foundation for a detailed exploration of afterglow emission physics in Section 3. Here, I focus on synchrotron radiation, the primary mechanism driving afterglow emission, and analyze the behaviour of afterglows across various surrounding environments and the intrinsic collimation of GRB jets. This section discusses constraining afterglow spectral and temporal parameters from observational data through analytical methods. Section 4 is dedicated to the correction of extinction in the GRB afterglow signal caused by the dust in galaxies, which I demonstrate by performing extinction correction on GRB 181110A, and in section 5, I apply the learned principles in modelling the GRB 230204B. Finally, Section 6 presents the conclusion and outlines future directions for this project.

# 1 Overview

## 1.1 What are Gamma Ray Bursts ?

Gamma Ray Bursts (GRBs) are the brightest and the most luminous explosions in the Universe, emitting intense flashes of gamma rays (Piran 2004). For their duration, they can outshine their entire host galaxies (Kumar and Zhang 2015). They were first detected by the Vela Satellites launched in the 1960s to monitor nuclear activity (Klebesadel, Strong, and Olson 1973). However, their extragalactic origins were confirmed much later (Metzger et al. 1997). Their isotropic distribution in the sky and vast luminosities fueled the initial skepticism towards extragalactic origins (Fishman and Meegan 1995), and the discovery of afterglows in 1997 and subsequent redshift measurements confirmed it (Paradijs et al. 1997).

The duration of a GRB is measured by their T90 value, which is the duration in which 5% and 95% of the total energy of the burst is emitted (Kouveliotou et al. 1993). Observationally, we find a bimodal distribution (Nakar 2007). Long GRBs, lasting more than 2 seconds, are typically associated with the collapse of massive stars (hypernovae Woosley and Bloom 2006). In contrast, short GRBs, lasting less than 2 seconds, are believed to result from the mergers of compact objects such as neutron stars (Berger 2014). Short GRBs tend to be harder than Long GRBs, where *hardness* is the ratio of the number of photons in the high-energy channel to the number of photons in the low-energy channel (Gehrels, Ramirez-Ruiz, and Fox 2009). The prompt emission is followed by a broadband emission called the afterglow (Meszaros 2006).

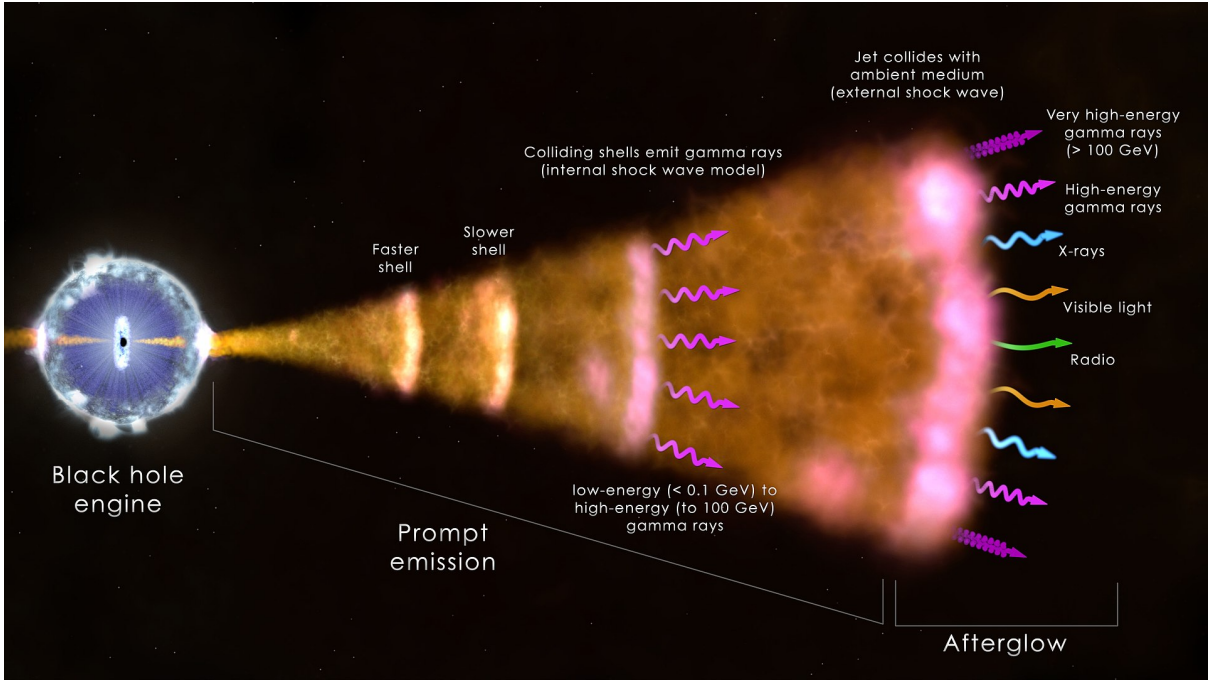


Figure 1: GRB Mechanism (Credit: NASA/Goddard Space Flight Center/ICRAR)

## 1.2 What are GRB Afterglows ?

The afterglow arises from the interaction of relativistic ejecta with the circumburst medium (Piran 2004). As the shockwave produced by the burst propagates outwards and decelerates, it accelerates the charged particles in the surrounding medium, causing them to emit radiation, primarily through the synchrotron process (Meszaros 2006). The afterglow emission is broadband emission; hence, it is detected across the electromagnetic spectrum, from x-rays to radio (Paradijs et al. 1997). The behavior of afterglow across different frequencies can be modelled using shock physics and the synchrotron emission theory, with the key frequencies (e.g. characteristic, peak and cooling) playing an essential role in determining the spectral and temporal properties of the afterglow emission (Sari, Piran, and Narayan 1998).

Afterglow observations and analysis provide insight into the structure and energy distribution of the relativistic jets, as well as the density and composition of the surrounding medium (Kumar and Zhang 2015). Optical observations help determine the redshift of the source (Metzger et al. 1997). Afterglows are visible weeks after the initial burst, offering astronomers an extended window to study the high-energy phenomenon involved in the burst.

## 1.3 Significance of studying GRBs

The field of GRBs is almost unique in astrophysics in its multi-disciplinary nature. Studying GRBs connects various fields in contemporary astrophysics: Supernova physics and accretion physics in stellar astronomy, shock physics, galactic astronomy and cosmology.

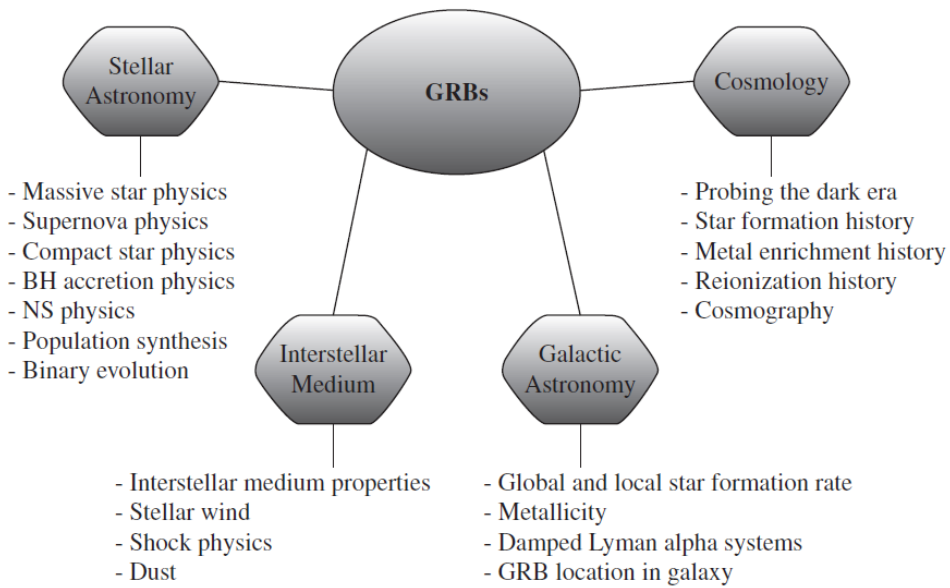


Figure 2: Flowchart from Zhang (2018) showing connection of GRBs with different fields in Astrophysics

## 2 Basic Theoretical Framework

### 2.1 Relativistic Motion

One of the coolest arguments for relativistic motion of GRB Jets towards earth is the *compactness problem*. Following the derivation and arguments in Zhang (2018), we observe that in gamma ray bursts, we detect gamma ray photons of energies greater than the rest mass energy of two electrons ( $\sim 1.02$  MeV). These photons can undergo the process of pair production, producing electron-positron pairs. For these electrons to escape the GRB source, the optical depth of the process should be less than unity. But, as I shall demonstrate, the optical depth of the process is much higher than unity, unless relativistic motion is invoked.

To order of magnitude, one may estimate the optical depth of pair production as

$$\tau_{\gamma\gamma} = \sigma_T n_{ph} R$$

where  $\sigma_T$  is the Thomson cross section,  $n_{ph}$  is the photon number density and  $R$  is the size of the emission region. In astronomy, we can get a good estimate of the size of the emission region by the time variability scale  $\delta t$ .

$$R = c\delta t$$

This is based on the consideration that an instantaneous signal emitted everywhere from the emitting region, will reach the observer with time spread of the order  $\delta t$ .

Consider a GRB with typical fluence

$$S_\gamma \sim 10^{-6} \text{ erg cm}^{-2}$$

at a luminosity distance

$$D_L \sim 2 \times 10^{28} \text{ cm},$$

which corresponds to a redshift of nearly 1. Therefore, the isotropic equivalent energy in the fireball is

$$E_{\gamma,iso} \sim 4\pi D_L^2 (1+z)^{-1} S_\gamma \sim 2.5 \times 10^{51} \text{ erg}.$$

Taking the time variability scale  $\delta t \sim 10$  ms, the typical size of emission region becomes  $c\delta t \sim 3 \times 10^8$  cm.

Assuming, that only a fraction  $f$  of the energy is emitted above the threshold for pair production, the number density of the photons becomes

$$n_{ph} \sim \frac{3E_{\gamma,iso}f}{4\pi R^2 \epsilon_\gamma} \sim (2.7 \times 10^{31} \text{ cm}^{-3}) f$$

Therefore, the optical depth becomes,

$$\tau_{\gamma\gamma} \sim \frac{3E_{\gamma,iso}\sigma_T f}{4\pi R^2 \epsilon_{gamma}} \sim 5.4 \times 10^{15} f \gg 1$$

We see that the optical depth is very high, hence gamma ray photons with energy  $>$  MeV cannot escape the GRB source. However, if the GRB outflow is moving towards earth with a Lorentz Factor of  $\Gamma$ , two effects come into play which reduce the optical depth.

The first effect is the increase in the threshold energy and the second is the increase in the size of the emission region. Taking these effects into account, we can calculate the ratio of optical depth in relativistic case to non-relativistic case as

$$\frac{\tau_{\gamma\gamma}(R)}{\tau_{\gamma\gamma}(NR)} = \Gamma^{2\beta-2}$$

where  $\beta$  is the power-law photon number spectrum. With a typical value of  $\beta = 2, 2$ ,  $\Gamma > 220$  solves the compactness with  $f = 0.2$

Now that we are convinced that GRBs have highly energetic relativistic jets, the next natural thing to do is to understand models which explain the GRB Mechanism. There are many different models to explain GRB mechanisms in literature, amongst which the fireball model (Piran 1999) is the most widely accepted. A full mathematical discussion of such models is not a part of this study, as it focuses on the afterglows. However, in the next section I have described qualitatively the highlighting features of the model.

## 2.2 Qualitative description of GRB Model

Following the phenomenological description of GRB mechanisms given by Zhang (2018) in chapter 2 of his book, "The Physics of Gamma Ray Bursts", GRBs occur when the progenitor undergoes a catastrophic event, resulting in a sudden release of the gravitational energy of the system. The event results in the formation of a central engine, which continuously powers an outflow for a certain duration of time, converting the gravitational energy (accreting systems) or spin energy (spin-down systems) into thermal energy or magnetic dissipation sites. The outflow is likely to be collimated in the case of GRBs. I will delve into a more robust discussion for evidence of collimation during the discussion of the Jet Effect in afterglows. The thermal energy of the jet is converted into kinetic energy, making the ejecta reach relativistic speeds. A fraction of the initial thermal energy is released as photons at the photosphere of the outflow. The jet's remaining kinetic energy and/or Poynting flux energy is dissipated internally within the jet and gets converted to the internal energy of the particles in internal shocks. A fraction of this internal energy is carried by electrons (determined by  $\epsilon_e$ ) and is entirely dissipated in the form of electromagnetic radiation, contributing to the non-thermal GRB prompt emission. Post the prompt emission phase, the relativistic outflow of the jet plunges into the external medium, and a shock propagates into the medium. Emission from these external emissions powers the long-lived broadband afterglow emission. Early on, a reverse shock propagates into the jet and crosses it. The "reverse shock" is a misnomer, as the shock still propagates forward in the observer frame and travels backwards only in the shock frame. The spatial range between the photosphere and the external medium is called the internal emission site of the GRB, and the prompt emission most likely originates in this region. The mechanism behind the prompt emission remains an open question. The primary radiation mechanism behind the afterglow emission is the synchrotron emission.

## 3 Afterglow Physics

We will now delve deeper into the physics of synchrotron emission as it essential in understanding the afterglow emission. We will first explore the physics of synchrotron emission and in the later sections we will understand how it relates to the spectrum

observed in afterglows. The section is based on the chapter 5 and 8 of Zhang (2018), Sari, Piran, and Narayan (1998) and Gao et al. (2013).

### 3.1 Synchrotron Radiation

Synchrotron radiation is the electromagnetic radiation emitted by a gyrating relativistic particle in a magnetic field. It is important to understand Synchrotron Radiation because it is the leading candidate for emission mechanism in prompt emission, and is widely accepted to power the GRB afterglow.

#### For a single particle

Without getting into the derivation for the form of synchrotron spectrum by a particle of charge  $q$ , mass  $m$ , and Lorentz factor  $\gamma$  gyrating in a magnetic field  $B$  with an incident angle  $\alpha$  with respect to the field, (cause its a lot a math, and is not relevant for discussion on afterglows), I look it up from Rybicki and Lightman (1979).

The spectrum is given by

$$P(\nu, \gamma) = \frac{\sqrt{3}q^3 B \sin\alpha}{mc^2} F\left(\frac{\nu}{\nu_{ch}}\right)$$

where,  $P(\nu, \gamma)$  is the energy emitted per unit time per unit frequency  $\nu$ .  $\nu_{ch}$  is the characteristic frequency given by

$$\nu_{ch} = \frac{3}{4\pi} \gamma^2 \frac{qB_\perp}{mc}$$

and the function  $F$  is given by this complicated formula in terms of the modified Bessel Function  $K_\alpha$  as

$$F(x) = x \int_x^\infty K_{\frac{5}{3}} \xi d\xi$$

reaching its maximum at  $F(0.29)$ . The asymptotic behavior of the function helps us get an idea of the behavior of  $P(\nu, \gamma)$

$$F(x) \sim \begin{cases} \frac{4\pi}{\sqrt{3}\Gamma(1/3)} \left(\frac{x}{2}\right)^{1/3} \sim 2.15x^{1/3}, & x \ll 1, \\ \left(\frac{\pi}{2}\right)^{1/2} x^{1/2} e^{-x} \sim 1.25x^{1/2} e^{-x}, & x \gg 1. \end{cases}$$

For lower frequencies,  $P$  increases as  $\nu^{\frac{1}{3}}$  and at higher frequencies, there is an exponential cutoff.

We can integrate  $P(\nu, \gamma)$  over  $\nu$  to get total power emitted by a particle as

$$P(\gamma) = 2\sigma_T c \gamma^2 \beta_\perp^2 U_B$$

where,  $U_B$  is the energy density in the magnetic field,  $\beta_\perp$  is the dimensionless perpendicular velocity and  $\sigma_T$  is the Thomson cross section mentioned before.

$$\sigma_T = \frac{8\pi}{3} \left(\frac{q^2}{mc^2}\right)^2$$

## Population of particles with Power Law distribution

Going from single to ensemble is just a matter of integration. For ensemble of particles between some minimum and maximum energy with power law distribution can be modelled as

$$N(\gamma)d\gamma = C_\gamma \gamma^{-p} d\gamma, \gamma_m < \gamma < \gamma_M$$

where,  $\gamma_m$  and  $\gamma_M$  are the minimum and maximum Lorentz factors of electron energy distribution respectively.

To get Power distribution as function of frequency, I perform the following integral

$$P_{\text{tot}}(\omega) = C \int_{\gamma_m}^{\gamma_M} P(\omega) \gamma^{-p} d\gamma \propto \int_{\gamma_m}^{\gamma_M} F\left(\frac{\omega}{\omega_c}\right) \gamma^{-p} d\gamma.$$

where,

I perform this integral in particular regime, it can be performed in the other regimes to get the behavior in other regimes. In the other two regimes, we can use asymptotic forms of  $F(x)$  to perform the integral easily and get approximate behavior. Perform change of variable to  $x = \frac{\nu}{\nu_{ch}}$  to get

$$P_{\text{tot}}(\nu) \propto \nu^{-(p-1)/2} \int_{x_1}^{x_2} F(x) x^{(p-3)/2} dx.$$

Therefore,

$$P_{\text{tot}}(\nu) \propto \nu^{-(p-1)/2}$$

Therefore for all frequencies(three different regimes), we have

$$F_\nu \propto \begin{cases} \nu^{1/3}, & \nu < \nu_m, \\ \nu^{-(p-1)/2}, & \nu_m < \nu < \nu_M, \\ \nu^{1/2} e^{-(\frac{\nu}{\nu_M})}, & \nu > \nu_M. \end{cases}$$

where,  $\nu_m$  and  $\nu_M$  are  $\frac{3}{4\pi} \gamma_m^2 \frac{qB_\perp}{mc}$  and  $\frac{3}{4\pi} \gamma_M^2 \frac{qB_\perp}{mc}$  respectively.

Besides,  $\nu_m$  and  $\nu_M$ , the other important frequency that plays a key role in determining the spectrum of synchrotron emission is the cooling frequency.

## Cooling Frequency

The radiating charged particles continuously lose their energy, or are being *cooled*. The characteristic timescale of the process can be estimated by dividing total energy with power radiated.

$$\tau(\gamma) = \frac{\gamma mc^2}{\frac{4}{3} \gamma^2 \sigma_T c \beta^2 U_B} = \frac{6\pi m_e c}{\gamma \sigma_T \beta^2 B^2}$$

Here, I have averaged  $\beta_\perp$  for random direction of magnetic field. It can be easily checked  $\langle \beta_\perp^2 \rangle = \frac{2}{3} \beta^2$

Therefore, at a particular time  $t$ , the Lorentz factor above which particles have lost most of their energy is called cooling Lorentz factor.

$$\gamma_c(t) \approx \frac{6\pi m_e c}{\sigma_T B^2 t}$$

where,  $\beta \sim 1$ .

## Time Evolution

Till now, we have discussed only static case of the synchrotron spectrum. In astrophysical systems, fresh particles are always getting accelerated by the shock travelling through the medium. In order to calculate the time evolution of the synchrotron spectrum, we need to take into the time dependence of energy distribution of electrons, taking into account injection of new particles, cooling and heating of old particles and diffusion of particles from source (Park and Petrosian 1995).

We will study the time dependent behavior by referring to Park and Petrosian (1995) and Zhang (2018). In case of GRBs, diffusion is negligible, and the continuity equation in energy space reduces to

$$\frac{\partial N(\gamma, t)}{\partial t} = -\frac{\partial}{\partial \gamma}[\dot{\gamma}(\gamma)N(\gamma, t)] + Q(\gamma, t)$$

where,  $\gamma_m$  and  $\gamma_M$  are the minimum *injection* Lorentz factor and maximum Lorentz factor respectively,  $N(\gamma, t)$  is the number of particles with energy between  $\gamma$  and  $\gamma + d\gamma$ ,  $\dot{\gamma}$  is the rate of change of energy of particles at a particular energy and  $Q(\gamma, t)$  is the source term. The behavior of source term can be assumed to be a power law as follows

$$Q(\gamma, t) \propto \left\{ \begin{array}{ll} [\frac{\gamma}{\gamma_m(t)}]^{-p}, & \gamma_m < \gamma < \gamma_M \end{array} \right.$$

One needs to numerically solve this equation to get solutions. But we can perform some order of magnitude approximate scalings to get the behavior of  $N(\gamma, t)$ . The scalings are as follows

$$\begin{aligned} \frac{\partial N(\gamma, t)}{\partial t} &\sim \frac{N}{t} \\ \dot{\gamma} \sim -\frac{\gamma}{\tau} &\implies -\frac{\partial}{\partial \gamma}[\dot{\gamma}(\gamma)N(\gamma, t)] \sim \frac{N}{\tau} \end{aligned}$$

Mostly in GRBs, we are concerned only with the slow cooling regime, where  $\gamma_m < \gamma_c$ . In the slow cooling regime, we can discuss the behavior of the two regimes of  $\gamma < \gamma_c$  and  $\gamma > \gamma_c$  as follows

- For  $\gamma_m < \gamma < \gamma_c < \gamma_M$ ,  $\tau \ll t$ , therefore, first term on RHS can be neglected, and we get  $N(\gamma, t) \sim \int Q(\gamma, t)dt \propto \gamma^{-p}$
- For  $\gamma_m < \gamma_c < \gamma < \gamma_M$ ,  $\tau \gg t$ , therefore, LHS is neglected and we get  $N \sim Q\tau \propto \gamma^{-p-1}$
- For  $\gamma < \gamma_m < \gamma_c < \gamma_M$ ,  $Q = 0$ , the first term on RHS can be neglected, and we see  $N(\gamma, t)$  has no explicit dependence on time, therefore the result from static case holds here.

Therefore, in slow cooling regime, we can write  $F_{nu}$  as

$$F_\nu \propto \begin{cases} \nu^{\frac{1}{3}}, & \nu < \nu_m < \nu_c < \nu_M \\ \nu^{\frac{-(p-1)}{2}}, & \nu_m < \nu < \nu_c < \nu_M \\ \nu^{\frac{-p}{2}}, & \nu_m < \nu_c < \nu < \nu_M \end{cases}$$

## Synchrotron Self Absorption

To complete the discussion of synchrotron spectrum in this study, we lastly discuss synchrotron self absorption. It is an important feature visible towards the lower frequencies in the spectrum and in radio lightcurves.

Below a certain frequency  $\nu_a$  called absorption frequency, the synchrotron flux is self absorbed, and the spectrum behaves like a blackbody spectrum, i.e.  $F_\nu \propto \nu^2$

Finally, we can express the synchrotron spectrum in a multi-segmented broken power law. I present the result published by Sari, Piran, and Narayan (1998).

$$F_{nu} = \begin{cases} \left(\frac{\nu_a}{\nu_m}\right)^{\frac{1}{3}} \left(\frac{\nu}{\nu_a}\right)^2, & \nu \leq \nu_a, \\ \left(\frac{\nu}{\nu_m}\right)^{\frac{1}{3}}, & \nu_a < \nu \leq \nu_m, \\ \left(\frac{\nu}{\nu_m}\right)^{-\frac{p-1}{2}}, & \nu_m < \nu \leq \nu_c, \\ \left(\frac{\nu_c}{\nu_m}\right)^{-\frac{p-1}{2}} \left(\frac{\nu}{\nu_c}\right)^{-\frac{p}{2}}, & \nu_c < \nu \leq \nu_M. \end{cases}$$

## 3.2 External Forward Shock Model

We now understand how we can reconstruct the synchrotron spectrum using a broken power law, given we have the knowledge of the characteristic frequencies, namely, absorption frequency, minimum injection frequency and the cooling frequency. To get the behavior of afterglow of the GRB, one needs to solve the relativistic hydrodynamical equations of an expanding fireball in the presence of magnetic fields (Meszaros 2006). Instead of focusing on the background math, we will look into the features of spectrum in different cases of external forward shock model. The afterglow flux is a function of frequency and time. We hereby, adopt the convention

$$F \propto \nu^{-\beta} t^{-\alpha}$$

The first step to investigate a GRB afterglow is almost always to investigate the relation between  $\alpha$  and  $\beta$ . The  $\alpha - \beta$  relations in different spectral regimes are called *closure relations*. The effectiveness of any GRB Model can be tested by confronting the model predictions with the closure relations.

The GRB afterglow is determined the following key parameters whose values are general conclusions from these analyses (Panaitescu and Kumar 2001; Panaitescu and Kumar 2002; Zhang et al. 2007; Gao et al. 2015; Yost et al. 2003; Zhang 2018) :

- $E_{K,iso,52}$  is the isotropic equivalent kinetic energy of the afterglow ( $\sim 10^{50}$ - $10^{54}$  ergs).
- $p$  is the power law index of the energy distribution of electrons ( $\sim 2$  -  $3$ ).
- $\theta_{\text{core}}$  is the jet opening angle of the jet. Its value can be derived only in the cases where the jet break is detected in the lightcurve ( $\sim 0.7$  -  $20$  degrees).
- $n_0$  is the number density of the ISM in cm-3 ( $\sim 0.1$  cm $^{-3}$ ) and  $A_*$  is the density parameter for stellar wind medium.
- $\epsilon_E$  is the fraction of thermal energy in electrons ( $\sim 0.1$ ).
- $\epsilon_B$  is the fraction of thermal energy in magnetic field ( $\sim 0.001$ ).

- $z$  is the redshift of the source and  $d_L$  is the luminosity distance of the source.

These parameters can determine the afterglow lightcurve and spectrum for a Tophat GRB Jet in both ISM and wind media. Tophat jet is the one in which the energy of the jet has no angular dependence. Energy is emitted uniformly over the entire cone. The behavior of afterglow jets with more complicated structures has also been modelled (Ryan et al. 2020), but in this study we limit ourselves to Tophat jets.

### Constant Energy ISM Model

In this section, we will discuss the Constant Energy ISM Model, which describes the deceleration of an adiabatic fireball without energy injection into a medium with constant density. Physically, the value of electron energy distribution index ( $p$ ) is greater than 2, hence we will limit our discussion to  $p > 2$  case.

For the  $p > 2$  case, the forward shock emission can be characterized as (Yost et al. 2003; Zhang et al. 2007)

$$\begin{aligned}\nu_m &= 3.3 \times 10^{12} \text{ Hz} \left( \frac{p-2}{p-1} \right)^2 (1+z)^{1/2} \epsilon_{B,-2}^{1/2} \epsilon_{e,-1}^2 E_{\text{K,iso},52}^{1/2} t_d^{-3/2}, \\ \nu_c &= 6.3 \times 10^{15} \text{ Hz} (1+z)^{-1/2} (1+Y)^{-2} \epsilon_{B,-2}^{-3/2} E_{\text{K,iso},52}^{-1/2} n^{-1} t_d^{-1/2}, \\ F_{\nu,\text{max}} &= 1.6 \text{ mJy} (1+z) D_{28}^{-2} \epsilon_{B,-2}^{1/2} E_{\text{K,iso},52}^{1/2} n^{1/2}.\end{aligned}$$

where, a new parameter  $Y$  has been introduced, called the *inverse Compton* parameter.

Behavior of the afterglow in different spectral regimes in slow cooling and the respective closure relations are as follows:

Frequency Range	Flux Density $F_\nu$	Temporal Decay Index $\alpha$	Spectral Index $\beta$
$\nu < \nu_m$	$F_\nu = F_{\nu,\text{max}} \left( \frac{\nu}{\nu_m} \right)^{1/3} \propto \nu^{1/3} t^{1/2}$	$\alpha = \frac{1}{2}$	$\beta = \frac{1}{3}$
$\nu_m < \nu < \nu_c$	$F_\nu = F_{\nu,\text{max}} \left( \frac{\nu}{\nu_m} \right)^{-(p-1)/2} \propto \nu^{-(p-1)/2} t^{-3(p-1)/4}$	$\alpha = \frac{3(p-1)}{4}$	$\beta = \frac{p-1}{2}$
$\nu > \nu_c$	$F_\nu = F_{\nu,\text{max}} \left( \frac{\nu_c}{\nu_m} \right)^{-(p-1)/2} \left( \frac{\nu}{\nu_c} \right)^{-p/2} \propto \nu^{-p/2} t^{-(3p-2)/4}$	$\alpha = \frac{3p-2}{4}$	$\beta = \frac{p}{2}$

Table 1: Flux density, temporal decay index, and spectral index in different frequency regimes.

In the spectrum, we can clearly see the energy decreases with time. The flux increases at lower frequencies because  $\nu_m$  has not passed those frequencies yet. In the lightcurve, I would like to highlight the cooling break in X-Ray regime, where the  $\nu_c$  passes the X-ray band and in the radio regime, we can observe the steady rise till  $\nu_m$  crosses the radio band.

We can perform the above analysis in case of wind media as well. In wind medium, the density is not constant but falls as  $n \propto r^{-k}$ . In case of red-giant stars, the value of  $k$  is 3/2 and is 2 in case of Wolf-Rayet stars. The results discussed in the next section are for Wolf-Rayet stars.

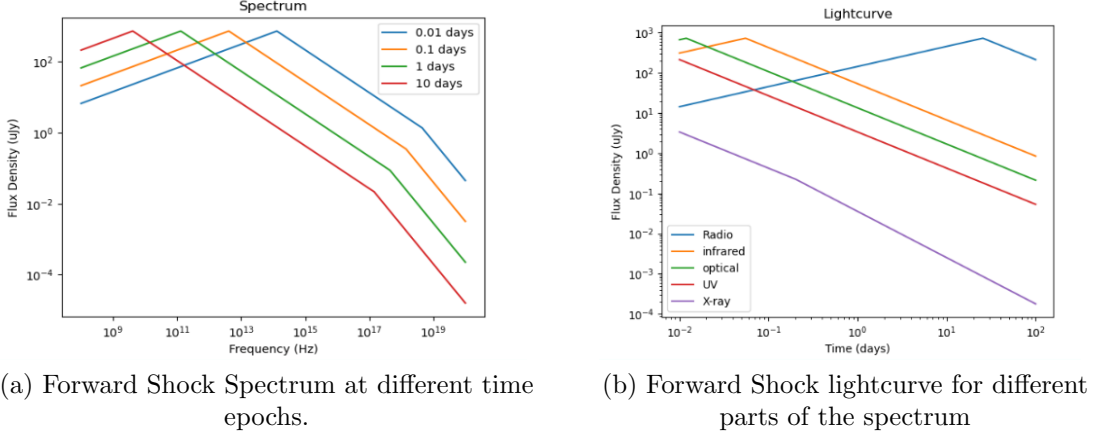


Figure 3: Spectrum(left) and lightcurve(right) of afterglow emission in case of constant energy jet in ISM environment

### Constant Energy Wind

For the  $p > 2$  case, the forward shock emission in the wind environment can be characterized as (Chevalier and Li 2000; Lü and Zhang 2014; Gao et al. 2013)

$$\begin{aligned} \nu_m &= 5.2 \times 10^{11} \text{ Hz} \left( \frac{p-2}{p-1} \right)^2 (1+z)^{1/2} \epsilon_{B,-2}^{1/2} \epsilon_{e,-1}^2 E_{\text{K,iso},52} t_d^{-3/2}, \\ \nu_c &= 1.7 \times 10^{18} \text{ Hz} (1+z)^{-3/2} (1+Y)^{-2} \epsilon_{B,-2}^{1/2} A_{*, -1}^{-2} E_{\text{K,iso},52}^{1/2} t_d^{1/2}, \\ F_{\nu,\max} &= 1.6 \text{ mJy} (1+z)^{3/2} \epsilon_{B,-2}^{-1/2} E_{\text{K,iso},52}^{1/2} t_d^{-1/2} A_{*, -1} d_{L,28}^{-2}, \end{aligned}$$

Behavior of the afterglow in different spectral regimes in slow cooling and the respective closure relations are as follows:

Frequency Range	Flux Density $F_\nu$	Temporal Decay Index $\alpha$	Spectral Index $\beta$
$\nu < \nu_m$	$F_\nu = F_{\nu,\max} \left( \frac{\nu}{\nu_m} \right)^{1/3} \propto \nu^{1/3}$	$\alpha = 0$	$\beta = -\frac{1}{3}$
$\nu_m < \nu < \nu_c$	$F_\nu = F_{\nu,\max} \left( \frac{\nu}{\nu_m} \right)^{-(p-1)/2} \propto \nu^{-(p-1)/2} t^{-(3p-1)/4}$	$\alpha = \frac{3p-1}{4}$	$\beta = \frac{p-1}{2}$
$\nu > \nu_c$	$F_\nu = F_{\nu,\max} \left( \frac{\nu_c}{\nu_m} \right)^{-(p-1)/2} \left( \frac{\nu}{\nu_c} \right)^{-p/2} \propto \nu^{-p/2} t^{-(3p-2)/4}$	$\alpha = \frac{3p-2}{4}$	$\beta = \frac{p}{2}$

Table 2: Flux density, temporal decay index, and spectral index for different frequency regimes.

In the spectrum, we can observe the constant flux in time before the  $\nu_m$  break, as curves at different epochs trace each other. This behavior is clearly evident in the lightcurve of radio wavelengths, as  $\nu_m$  crosses the radio band at much later times, the radio flux is constant before  $\nu_m$  break. The other key difference to be highlighted between wind and ISM environments is change in temporal evolutions of  $F_{\nu,\max}$  and  $\nu_c$ .  $F_{\nu,\max}$  goes from being constant in time to decreasing with time as  $F_{\nu,\max} \propto t^{-1/2}$  and  $\nu_c$  goes from decreasing with as  $t^{-1/2}$  to increasing with time as  $t^{1/2}$

### Closure Relations

In the above two subsections, we calculated the values of temporal index( $\alpha$ ) and spectral index( $\beta$ ) in different spectral regimes for constant energy (without energy injection) in

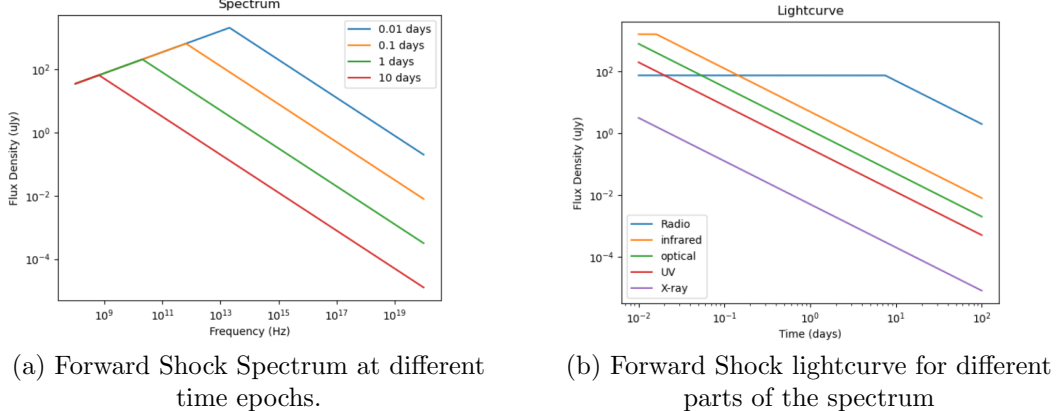


Figure 4: Spectrum(left) and lightcurve(right) of afterglow emission in case of constant energy jet in Wind environment

ISM and wind media. We can now relate  $\alpha$  and  $\beta$  to derive closure relations we talked about. Consistency with closure relations is one of the most basic checks we can perform to check the effectiveness of our GRB model. Although we derived them for only two of the cases, a complete list of closure relations can be found in literature addressing different scenarios in GRB afterglows. The following table has been taken from Racusin et al. (2009).

Closure Relations					
$\beta$	a No Energy Injection		b Energy Injection		
	$\alpha(\beta)$ ( $p > 2$ )	$\alpha(\beta)$ ( $1 < p < 2$ )	$\alpha(\beta)$ ( $p > 2$ )		
ISM, Slow Cooling					
1	$v_m < v < v_c$	$\frac{p-1}{2}$	$\alpha = \frac{3\beta}{2}$	$\alpha = \frac{3(2\beta+3)}{16}$	$\alpha = (q-1) + \frac{(2+q)\beta}{2}$
2	$v > v_c$	$\frac{p}{2}$	$\alpha = \frac{3\beta-1}{2}$	$\alpha = \frac{3\beta+5}{8}$	$\alpha = \frac{q-2}{2} + \frac{(2+q)\beta}{2}$
ISM, Fast Cooling					
3	$v_c < v < v_m$	$\frac{1}{2}$	$\alpha = \frac{\beta}{2}$	$\alpha = \frac{\beta}{2}$	$\alpha = (q-1) + \frac{(2-q)\beta}{2}$
4	$v > v_m$	$\frac{p}{2}$	$\alpha = \frac{3\beta-1}{2}$	$\alpha = \frac{3\beta+5}{8}$	$\alpha = \frac{q-2}{2} + \frac{(2+q)\beta}{2}$
Wind, Slow Cooling					
5	$v_m < v < v_c$	$\frac{p-1}{2}$	$\alpha = \frac{3\beta+1}{2}$	$\alpha = \frac{2\beta+9}{8}$	$\alpha = \frac{q}{2} + \frac{(2+q)\beta}{2}$
6	$v > v_c$	$\frac{p}{2}$	$\alpha = \frac{3\beta-1}{2}$	$\alpha = \frac{\beta+3}{4}$	$\alpha = \frac{q-2}{2} + \frac{(2+q)\beta}{2}$
Wind, Fast Cooling					
7	$v_c < v < v_m$	$\frac{1}{2}$	$\alpha = \frac{1-\beta}{2}$	$\alpha = \frac{1-\beta}{2}$	$\alpha = \frac{q}{2} - \frac{(2-q)\beta}{2}$
8	$v > v_m$	$\frac{p}{2}$	$\alpha = \frac{3\beta-1}{2}$	$\alpha = \frac{\beta+3}{4}$	$\alpha = \frac{q-2}{2} + \frac{(2+q)\beta}{2}$

Figure 5: Table of Closure Relations from Racusin et al. (2009)

### 3.3 Jet Effect

In this section, we will explore the effects the jet like structure of GRBs has on afterglow spectrum. To motivate the collimation of GRB Jets, we will start with a section which argues why GRB jets should be collimated, and in later sections we will see evidence in forms of key signatures in lightcurves that are best explained by collimated GRB jets. This entire section is based on chapter 8.4 of Zhang (2018).

## Arguments for collimation of GRB Jets

The isotropic equivalent energy from some of the GRBs is observed to be  $L_{\gamma,iso} \sim 10^{55}$  erg. For comparison, the rest mass energy of the Sun is nearly  $2 \times 10^{54}$  ergs. Theoretically, it is not possible to generate such high energy for a stellar explosion. With a beaming correction of  $f_b = (1 - \cos\theta)$ , the total energy output can be reduced to reasonable values.

$$E_\gamma = E_{\gamma,iso}(1 - \cos\theta)$$

Another conclusive argument for GRB jets to be collimated comes from the achromatic break observed in many GRB afterglows. This achromatic break is best explained by a collimated jet. I will explore this mechanism in detail in the following section.

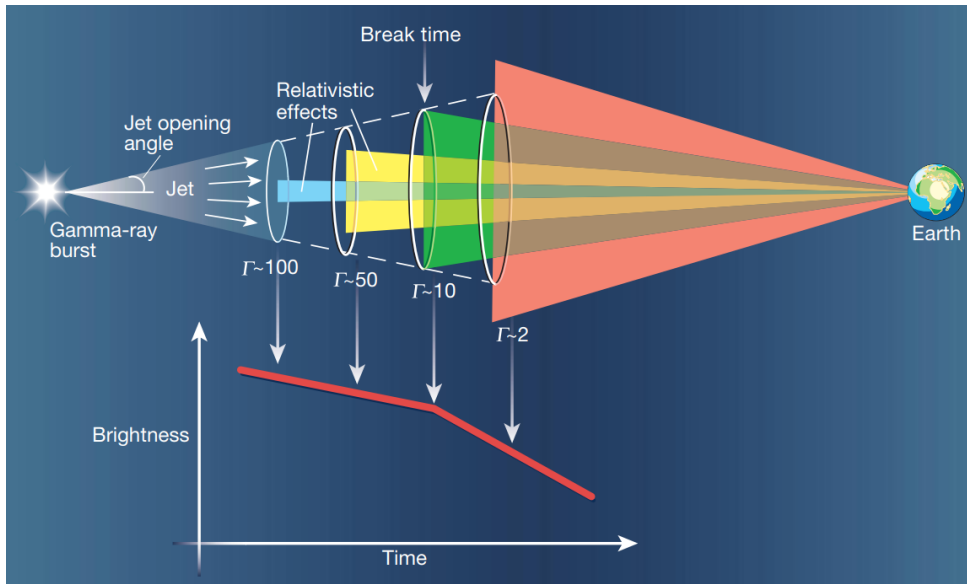


Figure 6: Schematic of a Jet Break by Woosley (2001)

## Principle of Jet Break

Consider a jet with an opening angle of  $\theta_j$ . Assume, the viewing angle is well within  $\theta_j$ . Due to relativistic beaming, we only observe flux from the  $\frac{1}{\Gamma}$  cone. As the blastwave decreases, the bulk Lorentz factor  $\Gamma$  of the jet decreases, increasing the emission cone. Jet break occurs when  $\frac{1}{\Gamma} \sim \theta_j$ , as the energy deficit outside the jet starts becoming noticeable. The effect manifests itself as steepening of the lightcurve.

The jet break in principle can arise from two effects: *edge effect* and *sideways expansion*.

### Edge Effect

This is purely a geometric effect. Before the jet break, ( $\Gamma^{-1} < \theta_j$ ), the observer has no knowledge of the collimation of the jet, as the emission dominantly comes from a cone of angle  $\frac{1}{\Gamma}$ .

Post jet break ( $\Gamma^{-1} > \theta_j$ ), the observer sees a deficit of energy from regions outside the jet, hence the lightcurve steepens from the isotropic case.

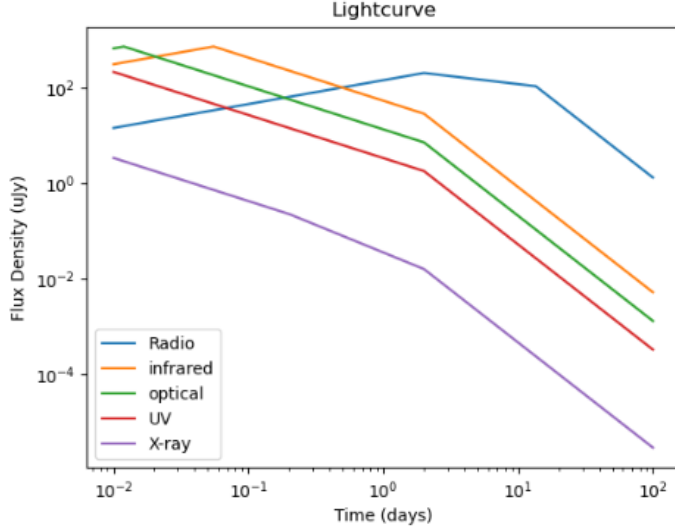


Figure 7: Lightcurve with a jet break at 2 days. We can observe the *achromatic* nature of the jet break, where in this ideal simulation it occurs simultaneously across all bands. Different slope for radio band is due to its different spectral regime

During the jet break, there is no change in the dynamics of the jet, as it is not a physical effect, but only a geometric effect. Hence the break is expected to be achromatic. The modification is

$$F_{\nu, \max} \propto t^{-0.75}$$

Therefore, solely due to edge effect, post jet break, the light curve steepens by 0.75, in case of ISM. Similarly in wind one has

$$F_{\nu, \max} \propto t^{-1}$$

In this case the steepening is by 0.5.

### Sideways Expansion

Rhoads (1999) and Sari, Piran, and Halpern (1999) considered the effect of sideways expansion of a conical jet, and suggested that it can further steepen the post-jet-break decay index.

For ISM, in *slow cooling* phase, they got the following results

$$F_{\nu} \propto \begin{cases} \nu^{1/3} t^{-1/3}, & \nu_a < \nu < \nu_m, \\ \nu^{-(p-1)/2} t^{-(p-1)}, & \nu_m \leq \nu < \nu_c, \\ \nu^{-p/2} t^{-p}, & \nu > \nu_c. \end{cases}$$

### 3.4 Reverse Shock Emission

Till now, we have discussed a system with a forward propagating shock only. In the early deceleration phase of the shock, as the forward shock plunges into the external medium, a reverse shock (reverse only in the ejecta frame, it still propagates forward in lab frame) propagates into the ejecta itself.

There are two distinct cases of reverse shock emission: thin shell and thick shell case. The thin shell cases and thick shell cases are differ from each other in the width of ejecta shell relative to the distance over which the ejecta decelerates.

In the thin shell case, the ejecta width is relatively narrow, hence the reverse shock propagates through the shell before significant deceleration of the entire shell occurs. This occurs when the shell is ejected at high Lorentz factors and encounters the external medium with sufficient density to slow it down. The reverse shock in this is typically mild and leads to short-lived, early-time afterglow emission (Sari and Piran 1995; Kobayashi, Piran, and Sari 1999).

Whereas, in the thick-shell case, the ejecta width is relatively high and reverse shock takes a longer time to propagate, giving time for jet to decelerate. This results in a longer and more intense reverse shock emission as reverse shock can propagate deeper within the shell. The thick shell case occurs when the shell is ejected at lower initial Lorentz factors or propagates into a lower-density medium (Zhang and Kobayashi 2005).

In this study we primarily focus on thin shells, motivated by the theoretical simplicity and its relevance to high Lorentz factor GRBs, which constitute a significant portion of observed GRBs. Including thick-shell models will introduce additional complexities which are beyond the current scope of analysis. Additionally, the reverse shock includes pre and post crossing phases. In this study, only post crossing phase is discussed. A complete analysis of reverse shocks, both thin and thick shells in pre and post crossing phases is more complex than simple external forward shock analysis and is one of the future goals of this project.

One key difference from forward shock that arises in the post crossing thin shell reverse shock case is that the cooling frequency  $\nu_c$  should be replaced by the cut-off frequency  $\nu_{\text{cut}}$ . This is because, after the shock crosses the shell, no new electrons are accelerated (Zhang 2018). The maximum electron energy  $\nu_M$  corresponds to  $\nu_{\text{cut}}$ , which is calculated by evolving  $\nu_c$  by the evolving cooling frequency by the end of shock crossing through adiabatic expansion (Kobayashi and Sari 2000). In this case, only slow cooling is possible, i.e.  $\nu_a < \nu_m < \nu_{\text{cut}}$  and  $\nu_m < \nu_a < \nu_{\text{cut}}$  (Zhang 2018).

$$\nu_{m,r} = (8.5 \times 10^{11} \text{ Hz}) z^{19/35} \frac{G(p)}{G(2.3)} E_{52}^{18/35} \Gamma_{0,2}^{-74/35} n_{0,0}^{-17/70} \epsilon_{e,-1}^2 \epsilon_{B,-2}^{1/2} t_2^{-54/35},$$

$$\nu_{\text{cut}} = (4.3 \times 10^{16} \text{ Hz}) z^{19/35} E_{52}^{-16/105} \Gamma_{0,2}^{-292/105} n_{0,0}^{-283/210} \epsilon_{B,-2}^{-3/2} t_2^{-54/35},$$

$$F_{\nu,\text{max},r} = (7.0 \times 10^5 \mu\text{Jy}) z^{69/35} E_{52}^{139/105} \Gamma_{0,2}^{-167/105} n_{0,0}^{37/210} \epsilon_{B,-2}^{1/2} D_{28}^{-2} t_2^{-34/35}.$$

Self-absorption frequency is different in two cases as:

$$\nu_{a,r} = (1.4 \times 10^{13} \text{ Hz}) z^{-73/175} \frac{g^{\text{XV}}(p)}{g^{\text{XV}}(2.3)} E_{52}^{69/175} \Gamma_{0,2}^{8/175} n_{0,0}^{71/175} \epsilon_{e,-1}^{1/5} \epsilon_{B,-2}^{-102/175} t_2^{-54/35},$$

for  $\nu_{a,r} < \nu_{m,r} < \nu_{c,r}$ .

$$\nu_{a,r} = (3.7 \times 10^{12} \text{ Hz}) z^{\frac{19p-36}{35(p+4)}} \frac{g^{\text{XVI}}(p)}{g^{\text{XVI}}(2.3)} E_{52}^{\frac{2(9p+29)}{35(p+4)}} \Gamma_{0,2}^{\frac{-74p+44}{35(p+4)}} n_{0,0}^{\frac{94-7p}{70(p+4)}} \epsilon_{e,-1}^{\frac{2(p-1)}{p+4}} \epsilon_{B,-2}^{\frac{p+2}{2(p+4)}} t_2^{\frac{54p+104}{35(p+4)}},$$

for  $\nu_{m,r} < \nu_{a,r} < \nu_{c,r}$ .

The functions  $g^{\text{XV}}(p)$ ,  $g^{\text{XVI}}(p)$ , and  $G(p)$  are defined as follows:

$$g^{\text{XV}}(p) = \frac{(p-1)}{(p-2)}(p+1)^{3/5}f(p)^{3/5},$$

$$g^{\text{XVI}}(p) = 8.3 \times 10^{-22} \left(\frac{p-2}{p-1}\right)^{\frac{2(p-1)}{p+4}} (p+1)^{\frac{2}{p+4}} f(p)^{\frac{p}{p+4}},$$

$$G(p) = \left(\frac{p-2}{p-1}\right)^2,$$

$$f(p) = \frac{\Gamma\left(\frac{3p+22}{12}\right)\Gamma\left(\frac{3p+2}{12}\right)}{\Gamma\left(\frac{3p+19}{12}\right)\Gamma\left(\frac{3p-1}{12}\right)}.$$

#### Four types of early optical lightcurves

Zhang (2018) discusses 4 types of early optical lightcurves in his book. The diagram in the book is presented in figure 8. In this subsection we will discuss a brief account of each of these lightcurves.

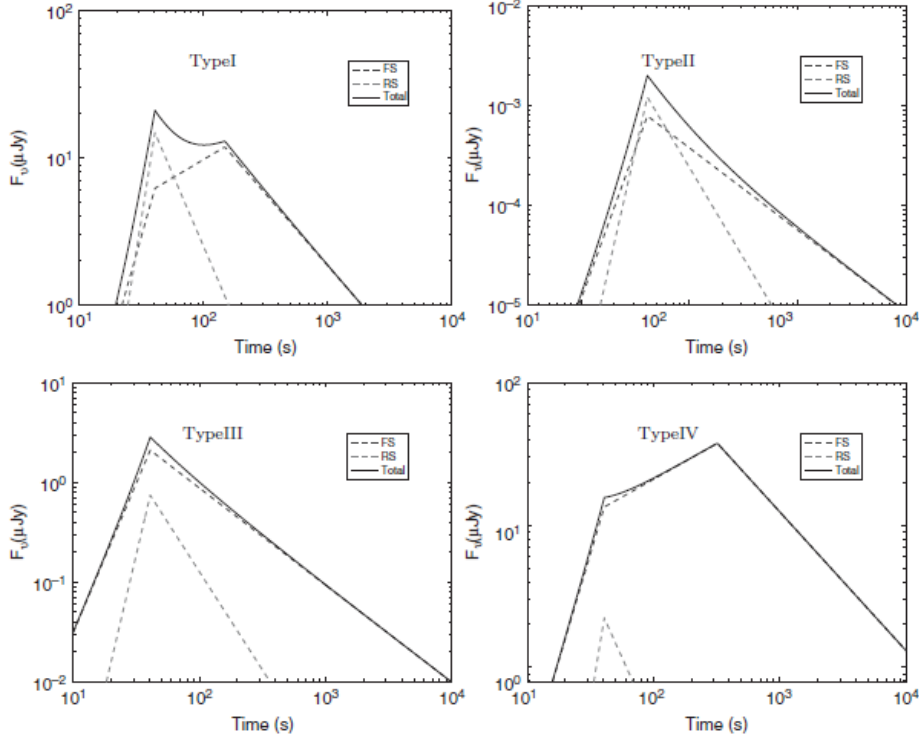


Figure 8: Four types of early optical lightcurves (Zhang 2018)

- Type I: Initially, the lightcurve is dominated by the reverse shock, characterized by steep rise and decay, but *re-brightening* occurs as the forward shock starts dominating and final decay phase occurs when  $\nu_m$  crosses the frequency band.

- Type II: In this case, the lightcurve shows the characteristic transition from  $\sim t^{-2}$  to  $\sim t^{-1}$  as seen in GRB 990123 (Akerlof et al. 1999) and many other GRBs. Like the previous case, the lightcurve is initially dominated by reverse shock and later transitions to forward shock dominated phase, but the difference being that  $\nu_m$  has already passed through the band before forward shock starts dominating.

- Type III & IV: In these cases, no reverse shock component is observed.

I simulated the reverse shock lightcurves taking the typical values for the parameters. The results for lightcurves in different bands are presented in figure 9, with a brief discussion of each lightcurve below.

- *X-Ray lightcurve*: No re-brightening is observed in the lightcurve, with reverse shock dominating very early and soon forward shock starting dominating. An interesting feature to observe is that the break due to the passing of cut-off frequency from the x-ray band in reverse shock is visible.
- *Ultraviolet lightcurve*: The lightcurve in this regime looks very similar to the type-II optical lightcurve, with the characteristic transition from  $\sim t^{-2}$  to  $\sim t^{-1}$ . The  $\nu_m$  break occurs later when forward shock starts dominating

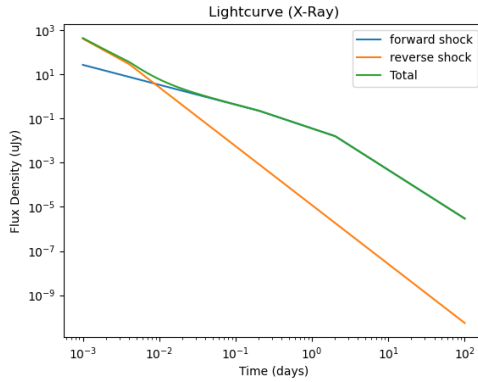


Figure 9: X-ray lightcurve

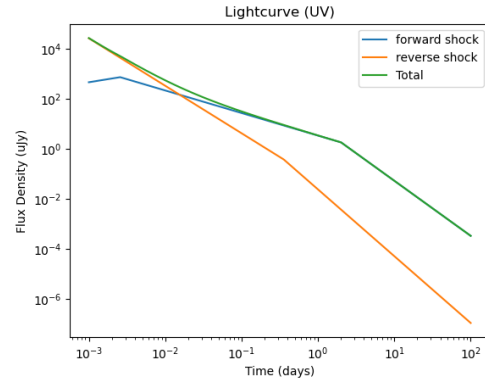


Figure 10: UV lightcurve

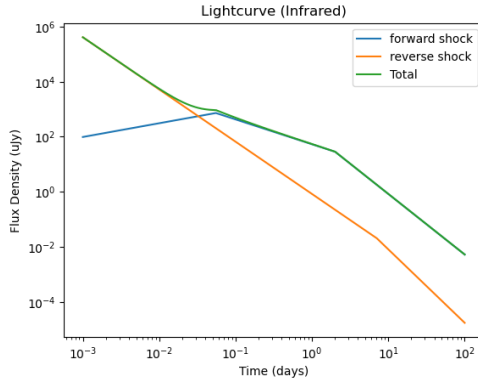


Figure 11: Infrared lightcurve

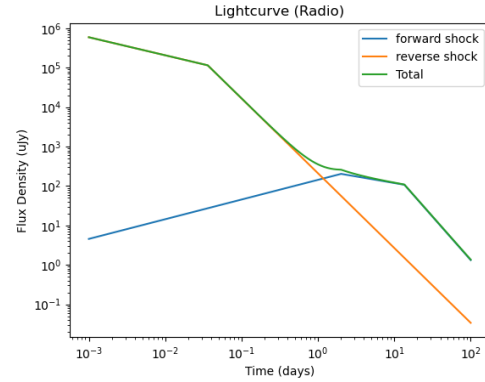


Figure 12: Radio Lightcurve

Figure 13: Early to late-time lightcurves for different frequencies.

- *Infrared lightcurve*: The lightcurve in this regime is similar to type-I optical in the sense that there is re-brightening in the lightcurve as the forward shock starts dominating. The  $\nu_m$  and  $\nu_c$  breaks from forward shock are observed later in the lightcurve while the break in the reverse shock remains hidden due to relatively low flux density of reverse shock.
- *Radio lightcurve*: The radio lightcurve shown here is an idealisation for theoretical completion. Most of the early-time features shown in the lightcurve will not be visible due to self-absorption. However, an interesting feature to notice is how reverse shock dominates for a longer duration of time in radio, and forward shock takes over only much later.

This concludes are brief discussion of thin shell post crossing reverse shock in ISM. A more complete study of reverse shocks is one of the future goals of the project. Studying reverse shocks is important to make sense of early afterglow data in many GRBs (GRB 130427A (Perley et al. 2014), GRB 140102A (Gupta et al. 2021) to name a few).

### 3.5 Model Parameter Constraints

In this section we will see how we can analytically relate and constrain some of the parameters governing the GRB afterglow spectrum. This is important because, before we run MCMC (Markov Chain Monte Carlo) simulations to find models with highest likelihood given our data, we must give appropriate priors and prior ranges. For some of the parameters, these can be done analytically and hence, can greatly reduce the parameter space to be sampled. This makes MCMC run more efficient and more likely to converge. Moreover, these analytical relations can be used as consistency checks for the model.

Under the framework of the external forward shock, there are six fundamental parameters: the isotropic kinetic energy  $E_{\text{K,iso}}$ , the density parameter ( $n$  for ISM or  $A$  for wind media), the jet opening angle  $\theta_{\text{core}}$  and the microphysics parameters ( $\epsilon_E$ ,  $\epsilon_B$  and  $p$ ) (Zhang 2018).

The jet opening angle enter the picture only when the jet break is observed in afterglow lightcurves (discussed in section 3.3). The relation as given in Zhang (2018) is

$$\theta_j \simeq (0.063 \text{ rad}) \left( \frac{t_j}{1 \text{ day}} \right)^{3/8} \left( \frac{1+z}{2} \right)^{-3/8} \left( \frac{E_{\gamma,\text{iso}}}{10^{53} \text{ erg}} \right)^{-1/8} \left( \frac{\tilde{\eta}_\gamma}{0.2} \right)^{1/8} \left( \frac{n}{0.1 \text{ cm}^{-3}} \right)^{1/8}$$

where,  $\tilde{\eta}_\gamma = \frac{E_{\gamma,\text{iso}}}{E_{\text{K,iso}}}$ . The electron energy distribution index  $p$  can be directly obtained from the slope of spectrum, once the spectral regime is known. One can know the spectral regime by checking consistency with the slopes of lightcurve and spectrum by using closure relations.

The other 4 parameters need to be constrained by fitting the data with afterglow model. We generally use, MCMC sampling to find the model with highest likelihood given the data.

However, in some cases, we can estimate  $E_{\text{K,iso}}$ . Freedman and Waxman (2001) showed that, for  $\nu \gg \nu_c$ ,  $\epsilon_E E_{\text{K,iso}}$  is given by

$$\epsilon_E E = (C_2 C_3)^{-1/2} C_1^{-1} \frac{d_L^2}{1+z} \nu t f_\nu(v, t) Y^\epsilon,$$

where

$$Y \equiv C_1 C_3^{1/2} C_2^{-3/2} \epsilon_E^{-3} \epsilon_B^{-1} d_L^{-2} \nu t f_\nu^{-1}(v, t), \quad \epsilon \equiv \frac{p-2}{p+2},$$

$$C_1 = 1.4 \times 10^{-21} \text{ cm}^{\frac{3}{2}},$$

$$C_2 = 6.1 \times 10^{-5} \text{ s}^{\frac{3}{2}} \text{ g}^{-\frac{1}{2}} \text{ cm}^{-1}$$

$$C_3 = 6.9 \times 10^{39} \text{ s}^{-\frac{3}{2}} \text{ g}^{-\frac{1}{2}} \text{ cm}^{-2}$$

Typically  $\epsilon_E$  is not too small ( $\sim 0.1$ ), hence from above, we can get a good measure of  $E_{\text{K,iso}}$  when we have observations for  $\nu \gg \nu_c$ .

## 4 Extinction Effects

By now we understand how studying characteristics of the afterglow are essential in understanding of physical processes underlying these high energy explosions. However, as the light travels from the source towards us, it encounters a lot of gas and dust which exists in galaxies and interstellar space. These extinction effects can obscure the observed light, making it important to apply the corrections to obtain accurate measurements of intrinsic emission of the source. In this section, we explore the nature of extinction effects and the methods used to correct for them. As an example, we will perform extinction correction on GRB 181110A. The theory of this section is based on Li et al. (2008) and the analysis of GRB 181110A is performed on the lines of Han et al. (2022).

### 4.1 What is extinction?

Extinction is absorption and scattering of electromagnetic radiation from gas and dust between an emitting body and an observer. In addition to extinction due to the Milky Way foreground, GRB afterglows face extinction due to the gas and dust in the host galaxy as well. There are two primary effects observed in GRBs due to extinction.

- *Dark Bursts* : There are examples of GRB afterglows, where emission was detected in X-Ray and Radio, but no or very little emission was observed in the optical. A very natural explanation for so called *dark bursts* is that the significant portion of the source is obscured by a dust column in their host galaxies.
- *Reddening* : Some GRBs with lower redshifts, appear very red due to extinction effects, which preferentially removes higher energy photons from the spectrum, leaving behind photons of longer wavelengths.

Studying extinction becomes very important in case of GRBs because it is crucial to correct for extinction in GRB afterglows to derive their intrinsic luminosities. It also helps constrain the nature of progenitors, for if long GRBs are formed from collapse of supermassive stars, it is very likely their optical and near-IR afterglows will suffer significant attenuation due to star forming molecular clouds in their environment. Extinction in GRBs helps probe the interstellar medium of high redshift galaxies, and hence helps us understand the star formation history of the Universe.

## 4.2 Formulation and Host Galaxy Correction

The amount of extinction and the wavelength dependence of extinction is described the following

$$F_\nu = F_o \left( \frac{\nu}{\text{Hz}} \right)^{-\beta} \exp \left[ -\frac{A_{V_r}}{1.086} \frac{A_{(1+z)\nu}}{A_{V_r}} \right]$$

where,  $F_o$  is the normalization constant,  $\beta$  is the intrinsic slope of the power law,  $z$  is the redshift of the source and  $A_{(1+z)\nu}$  is the extinction (in magnitudes) in the rest frame.

To correct for host galaxy extinction, I fit the data with the above law and determine the value of  $A_V$ . The value of  $A_V$  is related to the value of  $A_\lambda$  with the following formula

$$\begin{aligned} \frac{A_\lambda}{A_V} = & \frac{c_1}{(\lambda/0.08)^2 + (0.08/\lambda)^2 + c_3} \\ & + \frac{233 \left[ 1 - \frac{c_1}{6.88^2 + 0.145\lambda^2 + c_3} - \frac{c_4}{4.60} \right]}{(\lambda/0.046)^2 + (0.046/\lambda)^2 + 90} \\ & + \frac{c_4}{(\lambda/0.2175)^2 + (0.2175/\lambda)^2 - 1.95} \end{aligned}$$

Ideally, we should fit all the parameters namely,  $c_1$ ,  $c_2$ ,  $c_3$ ,  $c_4$  and  $A_V$ . However, in literature, there exist fits to the known extinction curves and we have derived values of  $c_1$ ,  $c_2$ ,  $c_3$  and  $c_4$ . These are often adopted as "templates" in GRB afterglow spectrum modelling. An important point to keep in mind is that all these models are valid only in Optical and UV. In X-rays, extinction modelling is different and is not discussed here. The unabsorbed (corrected) X-ray fluxes in case of Swift XRT are directly provided in their data products. The table for fitted values from Li et al. (2008) and the corresponding extinction curves are given below.

Extinction Curve	$c_1$	$c_2$	$c_3$	$c_4$	$\chi^2/\text{dof}$
MW .....	14.4	6.52	2.04	0.0519	1.66
LMC .....	4.47	2.39	-0.988	0.0221	1.19
SMC .....	38.7	3.83	6.34	0	1.36
Linear .....	66.2	4.97	22.1	0	1.42
Calzetti .....	44.9	7.56	61.2	0	1.68

Figure 14: Fits to known extinction curves

### The 2175 - angstrom feature

One of the most prominent features in extinction curve of Milky Way and to some extent in LMC is the bump around 2175 angstroms. This bump is completely absent in the curve of SMC. This bump was first observed in 1960s, but its origin is still not well understood.

## 4.3 Correcting for Galactic Extinction

Galactic extinction is dimming of light from distant sources due to dust and gas in the Milky Way. The extinction due to Milky Way does not require any fitting. I can use

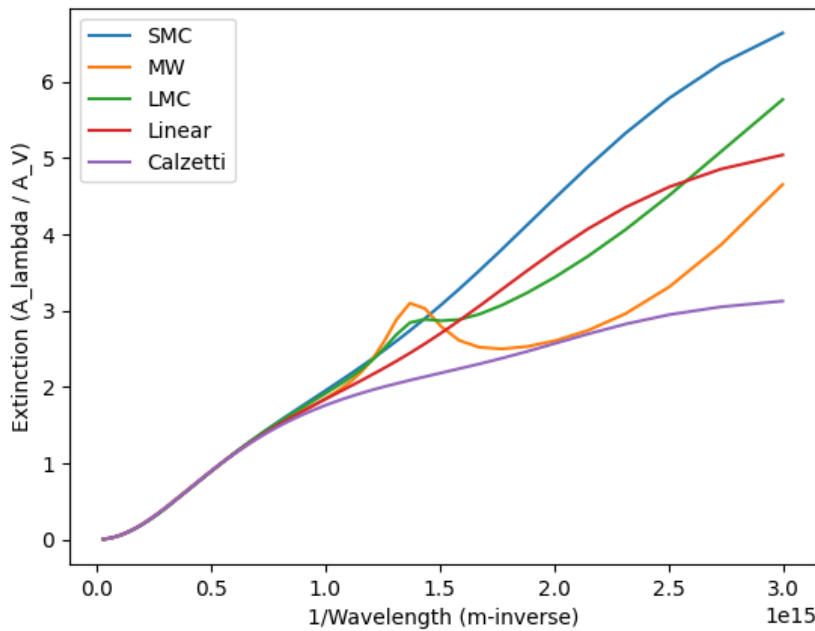


Figure 15: Different Extinction Models

dust maps to correct for Milky Way extinction. I can use the dust map to calculate the extinction from Milky Way along a particular line of sight.

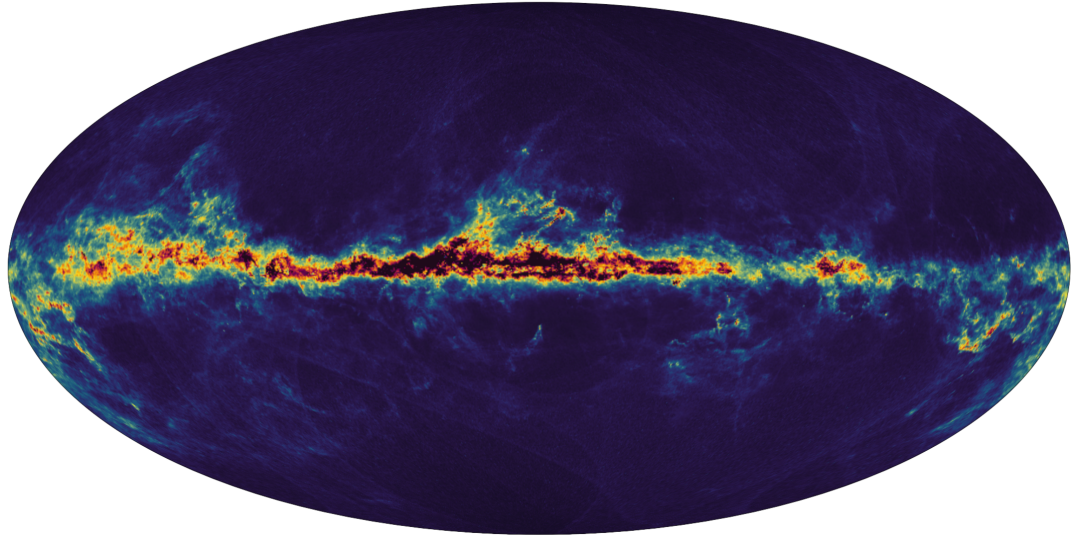


Figure 16: Dust Map of Milky Way created by ESA/Gaia/DPAC; CC BY-SA 3.0 IGO

The dust maps give us the value of color excess  $E(B - V)$ . It measures reddening as it calculates the difference between extinction B and V filters.  $E(B - V)$  is related to extinction in V band as

$$R_V = \frac{A_\lambda}{E(B - V)}$$

where,  $R_V$  is the ratio of total extinction V band to color excess between B and V bands. The typical value of  $R_V$  for Milky Way is 3.1. The value can be different for different regions in the galaxy, but we generally take the typical value of 3.1 for calculations.

#### 4.4 Extinction Correction in GRB 181110A

In this section I will present my work on correcting for extinction in the GRB 181110A. I have made use of the data supplied by the UK Swift Science Data Centre at the University of Leicester (Swift Burst Analyser). As in the paper (Han et al. 2022), I perform the analysis using the SED obtained at  $\sim 1400$  seconds after the  $T_0$  (time at which burst is detected) of the burst. The first step is to perform the line of sight Galactic Extinction. For galactic extinction correction, I directly take the value of  $E(B - V) = 0.0613$  given in the paper. The data corrected after the galactic extinction correction is present in figure 17. We see, after the galactic extinction has been corrected, the fluxes obtained

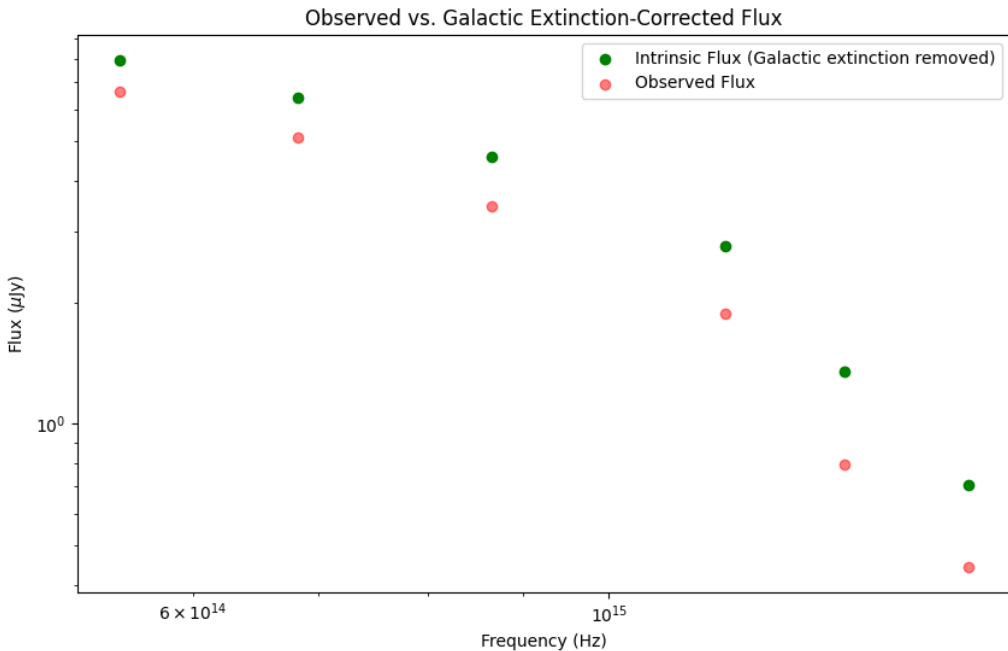


Figure 17: Log-Log plot of Correcting for Galactic Extinction in the SED obtained at  $T = 1400$ s after the  $T_0$  time of the burst

are higher as expected, with a higher correction towards the higher frequencies. Once we have corrected for Galactic Extinction, we can fit the extinction models discussed above to correct for Host Galaxy Extinction. Han et al. (2022) fit the afterglow SED with the Small Magellan Cloud (SMC) template extinction law and derive a small visual extinction ( $A_V = 0.09$ ), and find that the overall extinction law is consistent with a single power law with spectral slope  $\beta = 0.99$ . I find that the SED fits with Milky Way template extinction law better. I get the the value of extinction as  $A_V = 0.289$ . My fit is presented in the figure 18. Once we have fitted the Host Galaxy Extinction, we can correct for the host galaxy extinction by removing the calculated effects of host galaxy extinction at each frequency. In this case, post correction, I obtain a single power law in the Optical

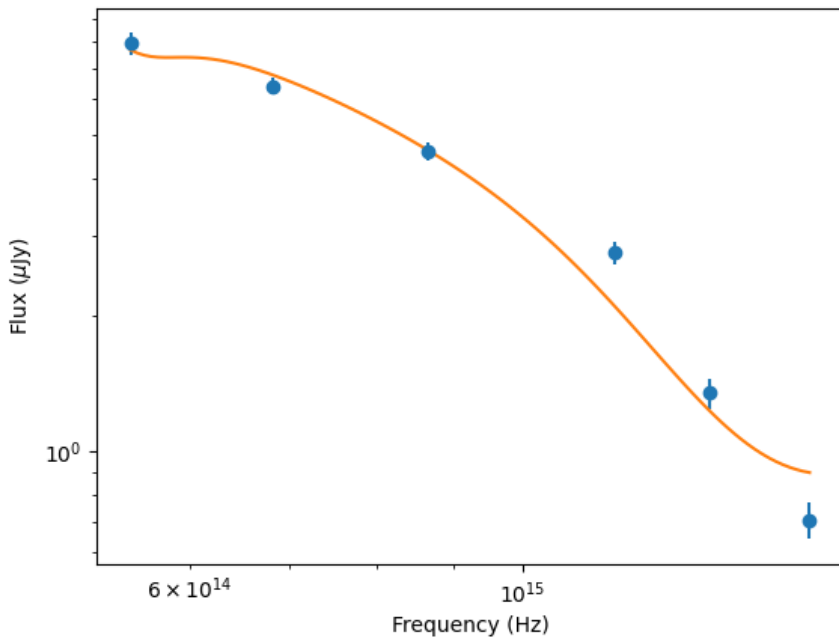


Figure 18: Log-Log plot of fit of observed flux with power law + Milky Way extinction template

to UV with spectral slope  $\beta_O = 1.31$ . The power law fit to Optical to UV spectrum is presented in the figure 19.

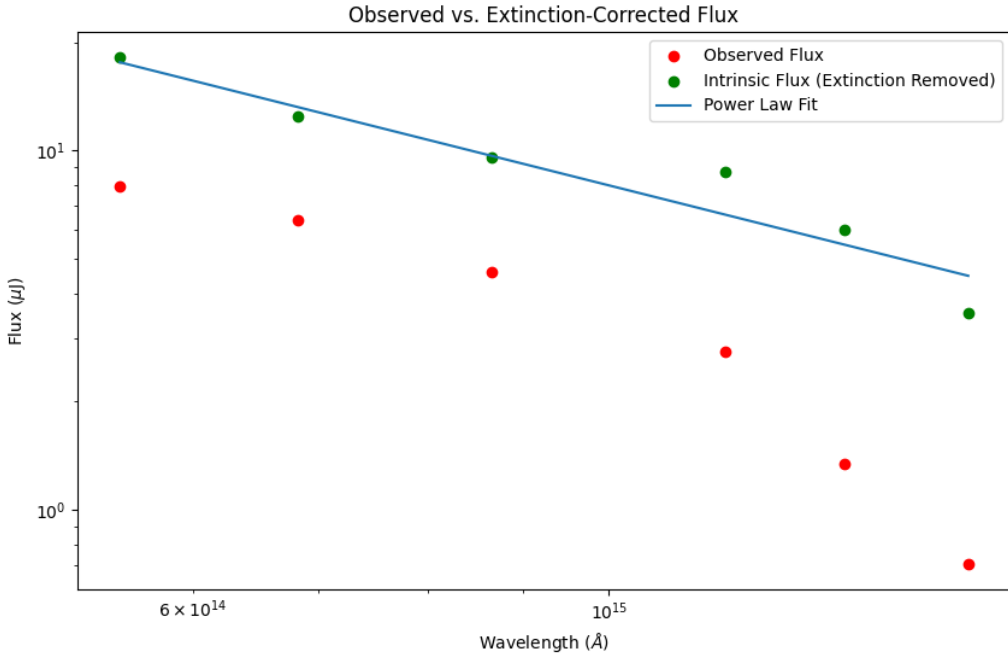


Figure 19: Log-Log plot of fitting power law to optical to UV SED. The fitted value of power law index  $\beta$  is 1.31

To compare the value of intrinsic spectral slope obtained by Han et al. (2022), I finally create a complete spectrum with corrected values in optical and UV by adding the unabsorbed XRT flux value at  $T_0 + 1398$  seconds. I fit a power law to this complete spectrum as shown in figure 20 and obtain  $\beta = 0.95$  with a standard deviation of  $\sigma = 0.03$ .

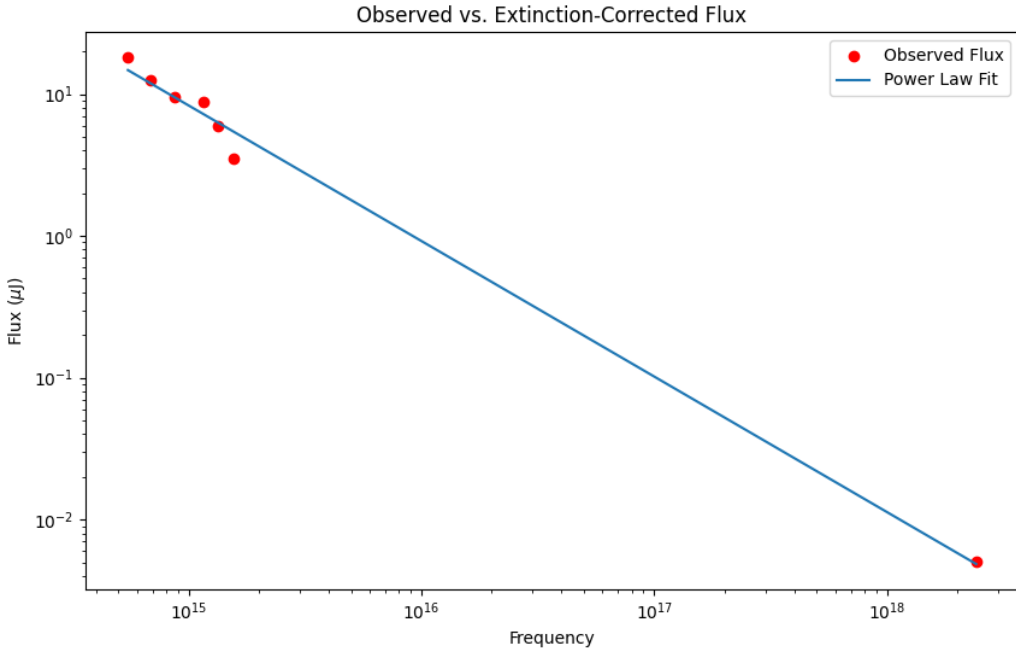


Figure 20: Log-Log plot of power law fit to overall spectrum from optical to X-ray

Finally, to summarise, I find Milky Way like extinction in the host galaxy with  $A_V = 0.289$ . Post-correction, I find that the overall spectrum from optical to X-ray is consistent with a single power law with spectral slope  $\beta = 0.95$ . I would like to thank Professor Varun Bhalerao for his help in this analysis.

## 5 Modeling of GRB 230204B

In this section, I would like to present the analysis of GRB 230204B conducted by Vishwajeet and I. Vishwajeet applied a single power law fit to the r-band data to extract the temporal power law decay index, which I have denoted as  $\alpha$ . With the extracted value of  $\alpha$  we applied closure relations to estimate the electron energy distribution index  $p$ . The temporal fit is present in figure 21 below.

### 5.1 Calculation of $p$ and ISM vs Wind Environment

With the extracted values of  $\alpha$ , we can solve for the value of  $p$  using the closure relations discussed in section 3.2. In ISM, The  $\nu < \nu_m$  is rejected simply because  $\alpha$  is 1.85, while  $\nu < \nu_m$  predicts  $\alpha = 0.5$  as discussed above. In wind case,  $\alpha = 0$  is expected theoretically, rejected this regime as well. In the  $\nu > \nu_c$  regime, in ISM case the relation is  $\alpha = \frac{3p-2}{4}$ , and we get the value of  $p = 3.13$ . In Wind, the relation is  $\alpha = \frac{3p-2}{4}$ , we again get the value of  $p = 3.13$ . The value of  $p > 3$  are very unlikely in GRBs, and hence we look for

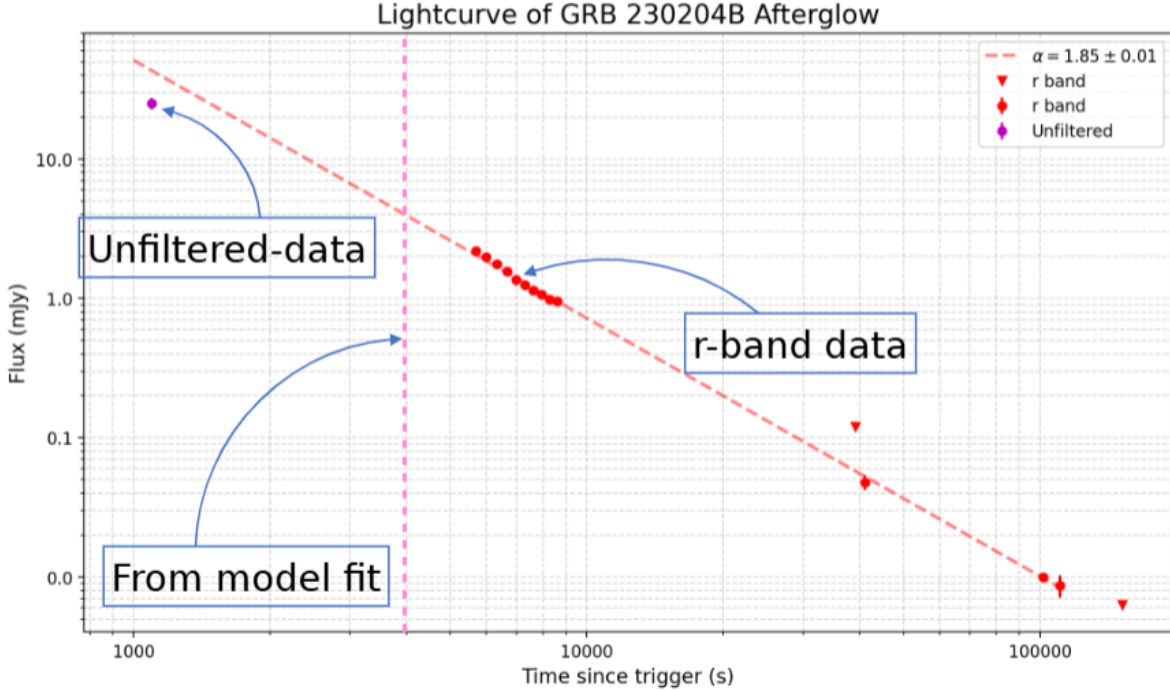


Figure 21: Power Law fit to r-band data. Credits : Vishwajeet (PhD student in STAR Lab, IITB)

more plausible values, if possible, in other regimes as well. In  $\nu_m < \nu < \nu_c$ , in ISM we get  $\alpha = \frac{3(p-1)}{4}$ , we get the value of  $\alpha = 3.46$ , and in case of wind, we have  $\alpha = \frac{3p-1}{4}$  and we get the value of  $p = 2.76$ . Hence, in wind for  $\nu_m < \nu < \nu_c$  we get a more plausible value for  $p$ .

### Observational Arguments for Wind

A justification for  $\nu_m < \nu < \nu_c$  regime in r-band and hence, another argument in the favor of  $p = 2.76$  is the characteristic  $F_\nu \propto t^0$  phase observed in radio for  $\nu < \nu_m$  regime. Hence observation in radio, are best explained by external forward shock model in Wind. Moreover, in wind case,  $\nu_c$  increases with time, hence its again very unlikely for  $\nu_c$  to have a low value of  $4.81 \times 10^{14}$  Hz (r-band frequency).

To summarise, the more feasible value of  $p = 2.76$  and the radio data suggest that it is likely that the GRB jet is expanding in a wind environment.

## 5.2 Forward Shock Model Fit and Parameter Extraction

With the wind environment identified as the more likely model, I fit the observed multi band data with forward shock model in wind using *dynesty* nested sampler. The results of fitting and the corners plots are presented in the figures 22 and 23 below, respectively. The fit is found to be consistent with the upper limits in data. The corner plots present the posterior distributions of the parameters, giving insights into parameter uncertainties and correlations. The values obtained for the fitted parameters are presented in Table 3.

The modelling of GRB 230204B is still an ongoing work. Further studies aim to improve upon the parameter estimation and studying the effect of jet opening angle on

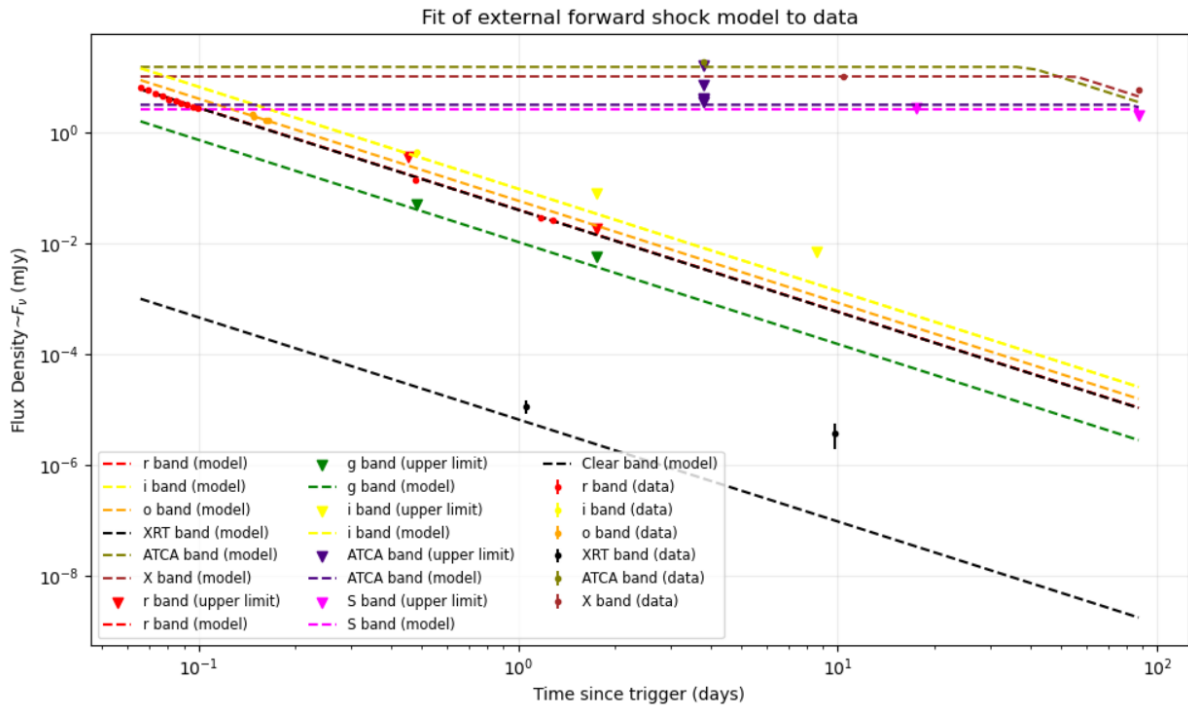


Figure 22: Fit of external forward shock model (wind) to the observed data

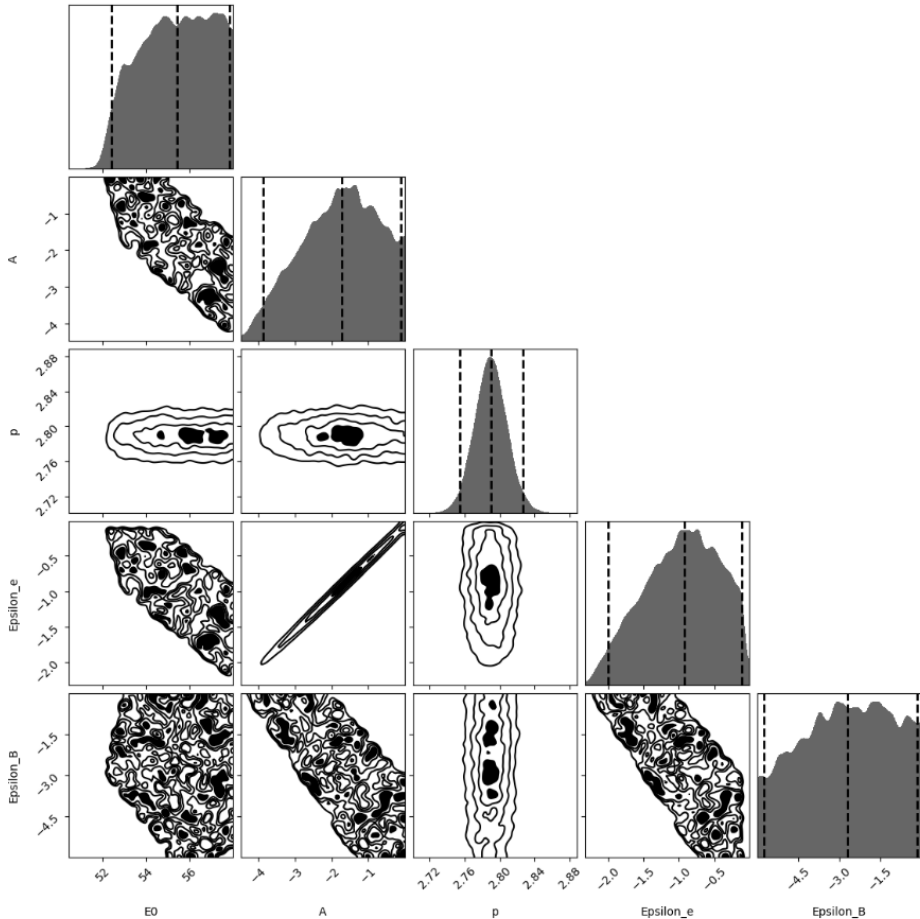


Figure 23: Corner Plots of Dynesty Run

Parameter	Value
$\log_{10} E_0$	$55.34 \pm 1.59$
$\log_{10} A$	$-1.79 \pm 1.03$
$p$	$2.78 \pm 0.02$
$\log_{10} \epsilon_e$	$-0.96 \pm 0.518$
$\log_{10} \epsilon_b$	$-2.76 \pm 1.62$

Table 3: Fitted parameters for GRB 230204B using the wind model.

the extracted parameters. Further studies also aim to provide additional constraints on the GRB environment, helping to confirm the wind medium hypothesis and offering a clearer understanding of the GRB’s afterglow evolution.

## 6 Conclusion

This report presents a theoretical and empirical study of gamma-ray burst (GRB) afterglows, aiming to understand the mechanisms behind these highly energetic bursts. I began this study by introducing GRBs and afterglows and highlighting their significance in broader fields of astrophysics. I then proceeded by arguing for the relativistic motion of GRB ejecta and a qualitative discussion of a GRB Model. Following this, I presented the basic principles of synchrotron radiation that underpin the afterglow emission. By modelling afterglow as synchrotron emission from electrons accelerated by the forward and reverse shocks, we explored how the properties of afterglows can be explained within both interstellar medium (ISM) and wind like environments. In addition to theoretical modelling of GRB afterglows, the report highlights the practical aspects of GRB analysis, including extinction effects that arise due to gas and dust in the host and Milky Way galaxy. Through a case study of GRB 181110A, I demonstrate how the observed afterglow data can be corrected for host as well as Milky Way extinction. In the final section, we applied these theoretical and analytical principles to model GRB 230204B. Through power law fitting and closure relations, we inferred that GRB most likely occurred in a wind like environment. Further, I fitted a forward shock model using dynesty nested sampler to gain insights into the microphysical conditions of the GRB and its consistency with the observed upper limits. This analysis, even though it is ongoing, shows the effectiveness of analytical models along with the statistical fitting for studying GRBs.

### 6.1 Future Work

The future work of this project includes a more comprehensive analysis of reverse shocks and completing the ongoing analysis of GRB 230204B with Vishwajeet and GRB 230812B with Utkarsh. The project will be extended to bulk analysis of GRB afterglows observed with the Growth India Telescope (GIT). The study of this larger dataset will enable a statistical study of afterglow properties and will provide a broader understanding of characteristics of GRB afterglows.

## Acknowledgments

I would like to thank Prof. Varun Bhalerao and his PhD students Vishwajeet Swain and Utkarsh Pathak for their guidance on this project.

# Bibliography

- Akerlof, C. et al. (Apr. 1999). “Observation of contemporaneous optical radiation from a gamma-ray burst”. In: *Nature* 398.6726, 400–402. ISSN: 1476-4687. DOI: 10.1038/18837. URL: <http://dx.doi.org/10.1038/18837>.
- Berger, E. (2014). “Short-duration gamma-ray bursts”. In: *Annual Review of Astronomy and Astrophysics* 52, pp. 43–105. DOI: 10.1146/annurev-astro-081913-035926.
- Chevalier, Roger A. and Zhi-Yun Li (June 2000). “Wind Interaction Models for Gamma-Ray Burst Afterglows: The Case for Two Types of Progenitors”. In: 536.1, pp. 195–212. DOI: 10.1086/308914. arXiv: [astro-ph/9908272 \[astro-ph\]](#).
- Fishman, G. J. and C. A. Meegan (1995). “Gamma-ray bursts”. In: *Annual Review of Astronomy and Astrophysics* 33, pp. 415–458. DOI: 10.1146/annurev.aa.33.090195.002215.
- Freedman, Deborah L. and Eli Waxman (Feb. 2001). “On the Energy of Gamma-Ray Bursts”. In: *The Astrophysical Journal* 547.2, 922–928. ISSN: 1538-4357. DOI: 10.1086/318386. URL: <http://dx.doi.org/10.1086/318386>.
- Gao, He et al. (2013). “A complete reference of the analytical synchrotron external shock models of gamma-ray bursts”. In: *New Astronomy Reviews* 57.6, pp. 141–190. ISSN: 1387-6473. DOI: <https://doi.org/10.1016/j.newar.2013.10.001>. URL: <https://www.sciencedirect.com/science/article/pii/S1387647313000171>.
- Gao, He et al. (Sept. 2015). “A MORPHOLOGICAL ANALYSIS OF GAMMA-RAY BURST EARLY-OPTICAL AFTERGLOWS”. In: *The Astrophysical Journal* 810.2, p. 160. ISSN: 1538-4357. DOI: 10.1088/0004-637x/810/2/160. URL: <http://dx.doi.org/10.1088/0004-637X/810/2/160>.
- Gehrels, N., E. Ramirez-Ruiz, and D. B. Fox (2009). “Gamma-ray bursts in the Swift era”. In: *Annual Review of Astronomy and Astrophysics* 47, pp. 567–617. DOI: 10.1146/annurev.astro.46.060407.145147.
- Gupta, Rahul et al. (May 2021). “GRB140102A: Insight into Prompt Spectral Evolution and Early Optical Afterglow Emission”. In: *Monthly Notices of the Royal Astronomical Society*.
- Han, Song et al. (Apr. 2022). “GRB 181110A: Constraining the Jet Structure, Circumburst Medium and the Initial Lorentz Factor”. In: *Universe* 8.4, 248, p. 248. DOI: 10.3390/universe8040248.
- Klebesadel, R. W., I. B. Strong, and R. A. Olson (1973). “Observations of gamma-ray bursts of cosmic origin”. In: *The Astrophysical Journal* 182, pp. L85–L88. DOI: 10.1086/181225.
- Kobayashi, S., T. Piran, and R. Sari (1999). “Can Internal Shocks Produce the Variability in GRBs?” In: *Astrophysical Journal* 513, pp. 669–678. DOI: 10.1086/306869.
- Kobayashi, Shiho and Re’em Sari (Oct. 2000). “Optical Flashes and Radio Flares in Gamma-Ray Burst Afterglow: Numerical Study”. In: 542.2, pp. 819–828. DOI: 10.1086/317021. arXiv: [astro-ph/9910241 \[astro-ph\]](#).
- Kouveliotou, C. et al. (1993). “Identification of two classes of gamma-ray bursts”. In: *The Astrophysical Journal* 413, pp. L101–L104. DOI: 10.1086/186969.
- Kumar, P. and B. Zhang (2015). “The physics of gamma-ray bursts & relativistic jets”. In: *Physics Reports* 561, pp. 1–109. DOI: 10.1016/j.physrep.2014.09.008.

- Li, Aigen et al. (Oct. 2008). “On Dust Extinction of Gamma-Ray Burst Host Galaxies”. In: *The Astrophysical Journal* 685.2, 1046–1051. ISSN: 1538-4357. DOI: 10.1086/591049. URL: <http://dx.doi.org/10.1086/591049>.
- Lü, Hou-Jun and Bing Zhang (Apr. 2014). “A Test of the Millisecond Magnetar Central Engine Model of Gamma-Ray Bursts with Swift Data”. In: 785.1, 74, p. 74. DOI: 10.1088/0004-637X/785/1/74. arXiv: 1401.1562 [astro-ph.HE].
- Meszaros, P. (2006). “Gamma-ray bursts”. In: *Reports on Progress in Physics* 69.8, pp. 2259–2322. DOI: 10.1088/0034-4885/69/8/R01.
- Metzger, M. R. et al. (1997). “Spectral constraints on the redshift of the optical counterpart to the  $\gamma$ -ray burst of 8 May 1997”. In: *Nature* 387.6636, pp. 878–880. DOI: 10.1038/43132.
- Nakar, E. (2007). “Short-hard gamma-ray bursts”. In: *Physics Reports* 442.1-6, pp. 166–236. DOI: 10.1016/j.physrep.2007.02.005.
- Panaitescu, A. and P. Kumar (Oct. 2001). “Fundamental Physical Parameters of Collimated Gamma-Ray Burst Afterglows”. In: *apjl* 560.1, pp. L49–L53. DOI: 10.1086/324061. arXiv: astro-ph/0108045 [astro-ph].
- (June 2002). “Properties of Relativistic Jets in Gamma-Ray Burst Afterglows”. In: 571.2, pp. 779–789. DOI: 10.1086/340094.
- Paradijs, J. van et al. (1997). “Transient optical emission from the error box of the  $\gamma$ -ray burst of 28 February 1997”. In: *Nature* 386.6626, pp. 686–689. DOI: 10.1038/386686a0.
- Park, Brian T. and Vahe Petrosian (June 1995). “Fokker-Planck Equations of Stochastic Acceleration: Green’s Functions and Boundary Conditions”. In: 446, p. 699. DOI: 10.1086/175828.
- Perley, D. A. et al. (Jan. 2014). “THE AFTERGLOW OF GRB 130427A FROM 1 TO 1016GHz”. In: *The Astrophysical Journal* 781.1, p. 37. ISSN: 1538-4357. DOI: 10.1088/0004-637x/781/1/37. URL: <http://dx.doi.org/10.1088/0004-637X/781/1/37>.
- Piran, T. (1999). “Gamma-ray bursts and the fireball model”. In: *Physics Reports* 314.6, pp. 575–667. DOI: 10.1016/S0370-1573(98)00127-6.
- (2004). “The physics of gamma-ray bursts”. In: *Reviews of Modern Physics* 76.4, pp. 1143–1210. DOI: 10.1103/RevModPhys.76.1143.
- Racusin, J. L. et al. (May 2009). “JET BREAKS AND ENERGETICS OF SWIFT GAMMA-RAY BURST X-RAY AFTERGLOWS”. In: *The Astrophysical Journal* 698.1, 43–74. ISSN: 1538-4357. DOI: 10.1088/0004-637x/698/1/43. URL: <http://dx.doi.org/10.1088/0004-637X/698/1/43>.
- Rhoads, James E. (Nov. 1999). “The Dynamics and Light Curves of Beamed Gamma-Ray Burst Afterglows”. In: 525.2, pp. 737–749. DOI: 10.1086/307907. arXiv: astro-ph/9903399 [astro-ph].
- Ryan, Geoffrey et al. (June 2020). “Gamma-Ray Burst Afterglows in the Multimessenger Era: Numerical Models and Closure Relations”. In: *The Astrophysical Journal* 896.2, p. 166. ISSN: 1538-4357. DOI: 10.3847/1538-4357/ab93cf. URL: <http://dx.doi.org/10.3847/1538-4357/ab93cf>.
- Rybicki, George B. and Alan P. Lightman (1979). *Radiative Processes in Astrophysics*. New York: Wiley.
- Sari, R. and T. Piran (1995). “Hydrodynamic Timescales and Temporal Structure of Gamma-Ray Bursts”. In: *Astrophysical Journal* 455, p. L143. DOI: 10.1086/309845.

- Sari, R., T. Piran, and R. Narayan (1998). “Spectra and light curves of gamma-ray burst afterglows”. In: *The Astrophysical Journal* 497.1, pp. L17–L20. doi: 10.1086/311269.
- Sari, Re’em, Tsvi Piran, and J. P. Halpern (July 1999). “Jets in Gamma-Ray Bursts”. In: *apjl* 519.1, pp. L17–L20. doi: 10.1086/312109. arXiv: astro-ph/9903339 [astro-ph].
- Woosley, S. E. and J. S. Bloom (2006). “The supernova  $\gamma$ -ray burst connection”. In: *Annual Review of Astronomy and Astrophysics* 44, pp. 507–556. doi: 10.1146/annurev.astro.43.072103.150558.
- Woosley, Stan (Dec. 2001). “Astronomy: Blinded by the light”. In: 414.6866, pp. 853–854. doi: 10.1038/414853a.
- Yost, S. A. et al. (Nov. 2003). “A Study of the Afterglows of Four Gamma-Ray Bursts: Constraining the Explosion and Fireball Model”. In: 597.1, pp. 459–473. doi: 10.1086/378288. arXiv: astro-ph/0307056 [astro-ph].
- Zhang, B. and S. Kobayashi (2005). “Gamma-Ray Burst Early Optical Afterglows: Reverse Shock Emission from an Arbitrarily Magnetized Ejecta”. In: *Astrophysical Journal* 628, pp. 315–334. doi: 10.1086/430486.
- Zhang, Bing (2018). *The Physics of Gamma-Ray Bursts*. Provided by the SAO/NASA Astrophysics Data System. Cambridge, UK: Cambridge University Press. doi: 10.1017/9781139226530. URL: <https://ui.adsabs.harvard.edu/abs/2018pgrb.book.....Z>.
- Zhang, Bing et al. (Feb. 2007). “GRB Radiative Efficiencies Derived from the Swift-Data: GRBs versus XRFs, Long versus Short”. In: *The Astrophysical Journal* 655.2, 989–1001. ISSN: 1538-4357. doi: 10.1086/510110. URL: <http://dx.doi.org/10.1086/510110>.